

A method for fine positioning of diagnostic packages in inertial confinement fusion experiments

Wei Wang, Tielin Shi, and Kok-Meng Lee

Citation: *Rev. Sci. Instrum.* **82**, 125113 (2011); doi: 10.1063/1.3669780

View online: <http://dx.doi.org/10.1063/1.3669780>

View Table of Contents: <http://rsi.aip.org/resource/1/RSINAK/v82/i12>

Published by the [American Institute of Physics](#).

Related Articles

Compensator design for improved counterbalancing in high speed atomic force microscopy
Rev. Sci. Instrum. **82**, 113712 (2011)

Compact x-ray microradiograph for in situ imaging of solidification processes: Bringing in situ x-ray micro-imaging from the synchrotron to the laboratory
Rev. Sci. Instrum. **82**, 105108 (2011)

Coded apertures allow high-energy x-ray phase contrast imaging with laboratory sources
J. Appl. Phys. **110**, 014906 (2011)

Three-view stereoscopy in dusty plasmas under microgravity: A calibration and reconstruction approach
Rev. Sci. Instrum. **82**, 053706 (2011)

Omnifocus video camera
Rev. Sci. Instrum. **82**, 045105 (2011)

Additional information on *Rev. Sci. Instrum.*

Journal Homepage: <http://rsi.aip.org>

Journal Information: http://rsi.aip.org/about/about_the_journal

Top downloads: http://rsi.aip.org/features/most_downloaded

Information for Authors: <http://rsi.aip.org/authors>

ADVERTISEMENT

**AIPAdvances**

Submit Now

**Explore AIP's new
open-access journal**

- **Article-level metrics
now available**
- **Join the conversation!
Rate & comment on articles**

A method for fine positioning of diagnostic packages in inertial confinement fusion experiments

Wei Wang,¹ Tielin Shi,¹ and Kok-Meng Lee^{1,2}

¹*School of Mechanical Science and Engineering, Huazhong University of Science and Technology, Wuhan 430074, China*

²*George W. Woodruff School of Mechanical Engineering, Georgia Institute of Technology, Atlanta, Georgia 30332, USA*

(Received 24 July 2011; accepted 23 November 2011; published online 29 December 2011)

A method based on binocular vision servoing for positioning of a diagnostic package in inertial confinement fusion (ICF) experiments is presented. The general diagnostic instrument manipulator will provide precision three dimension positioning and alignment-to-target capability in ICF experiments. In this work, we focus on the final precise automatic positioning with a binocular vision system. A three dimension image projection vector (IPV), which has an almost linear relationship with the target position in 3D space under the condition of weak perspective, is introduced to extract target position information from binocular image. The difference of the IPV between the current image and the desired image will be used as the input of servo controller. A differential motion model was found for the hybrid manipulator with three degrees of freedom. With this model and the said IPV, the servo strategy will be dramatically simplified compare with general image based visual servo in which the image Jacobian matrix needs estimated online. The experiment result implies that the locating accuracy of the manipulator is less than two pixels. This method can also be used in micromanipulation visual servo field. © 2011 American Institute of Physics. [doi:10.1063/1.3669780]

I. INTRODUCTION

When performing inertial confinement fusion (ICF) experiments, diagnostic instruments must be inserted and located at a precise position¹⁻⁵ in the target chamber. A vision-guided hybrid diagnostic instrument manipulator (DIM) providing three degrees of freedom (3-DOF), two rotational and one translational motion, has been designed for Shengguang Facility⁶ by Huazhong University of Science and Technology (HUST) in China for locating instruments with precision pointing and radial positioning. While functionally similar to the DIM at the National Ignition Facility (NIF),¹ the DIM discussed here is self-positioning guided by a coarse/fine vision system consisting of a large field-of-view (FOV) camera and a set of large magnification binocular cameras (LMBC) for the coarse and fine phases, respectively, so that a wide FOV can be achieved without sacrificing optical resolution. In coarse phase, the large-FOV camera tracks the target holder guiding the DIM to approach it. Once the target is within the FOV of the binocular cameras, the fine positioning phase begins. This paper introduces a new visual servo method for the three-DOF fine-positioning. Unlike most binocular vision algorithms where the depth information relies on knowledge of the two camera coordinate systems with respect to that of the target, the model presented here is axis-decoupled and linear reducing the visual servo problem to estimating the displacement between the desired and current positions of the diagnostic instrument. This model requires only an offline alignment of both cameras. Apart from eliminating the needs to perform *in situ* vision/manipulator calibration which are often tedious and costly, this method uses analytically computed control inputs to compensate for the displacement error, and thus dramatically reduces the number

of servo-loop iterations as compared to conventional control methods based on visual-servo-guided manipulator.

II. VISION-GUIDED MICRO-MOTION MANIPULATOR (V3M)

As shown in Fig. 1(a), the DIM is a 3DOF hybrid parallel/serial mechanism for positioning a cart assembly that houses the diagnostic instrument (DI) with associated utilities/cables and the coarse/fine vision guidance system. The DIM consists of a linear positioner translating the cart relative to the main tube and an extensible bipod providing pitch and yaw rotations. This kinematic design decouples the orientation pointing from the radial positioning of the DI.

Guided by the large-FOV vision system (mounted below the carrier cart, not shown) that bases images of the target holder, the 3-DOF manipulator approximately locates the target feature within the FOV of the LMBC with a pair of cameras mounted symmetrically on the carrier cart as shown in Fig. 2(a). Once the target is viewed in the LMBC, the fine positioning phase begins.

A. Offline alignment

Before placing the DIM in an ICF chamber in which experiments will be conducted, an offline vision system alignment is performed on a linear positioning stage with a mockup target (positioned on an adjustable 3-DOF stage) simulating the actual target in the ICF chamber as shown in Figs. 2(a) and 2(b). Mounted on the slider of the linear stage, the DI is placed on the cart such that its axis aligns with the slider motion. As an illustration, the tip of the DI is used as the datum

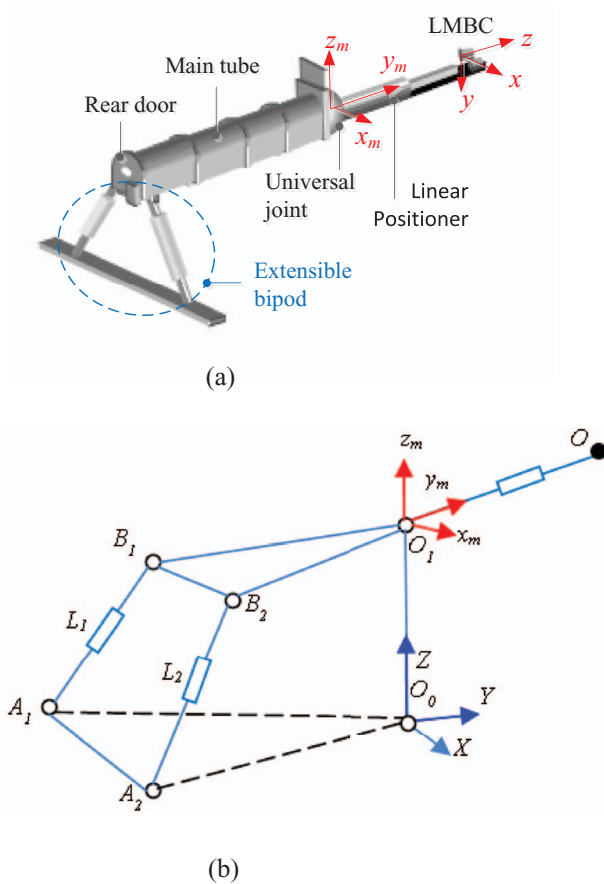


FIG. 1. (Color online) Diagnostic instrument manipulator (DIM). (a) Prototype V3M and (b) schematics illustrating the DIM kinematics.

for positioning the mockup target with the help of two orthogonally positioned microscopes. The alignment is performed in three steps: In step 1, the tip of the DI is positioned by the linear stage such that it coincides with the two microscopic axes as shown in Fig. 2(a). Gauged by the grating ruler as shown in Fig. 2(b), the DI is then retracted to the position (specified by the ICF experiment), which is followed by centering the mockup target at the position previously occupied by the tip of the DI during step 2. Once the mockup target is located, the binocular cameras are aligned such that the image points q_{\pm} of mockup target are the centers of the FOV as illustrated in Fig. 2(c), where the subscripts “+” and “-” refer to the right and left images, respectively. After the offline alignment procedure completes, the instruments and the camera will be immobilized on the cart.

The objective of the *in situ* binocular visual servo after inserting into the ICF chamber is to track the target p such that $p \rightarrow q$ where p and q are the binocular images of the actual and mockup, respectively. The remainder of this paper focuses on the fine motion phase with the LMBC.

B. Binocular vision system

Figure 2 illustrates the coordinate systems (following the right-hand rule) for the binocular vision system (BVS), where xyz is referred to here as BVS coordinate frame located at the midpoint between o_+ and o_- at which the two cameras

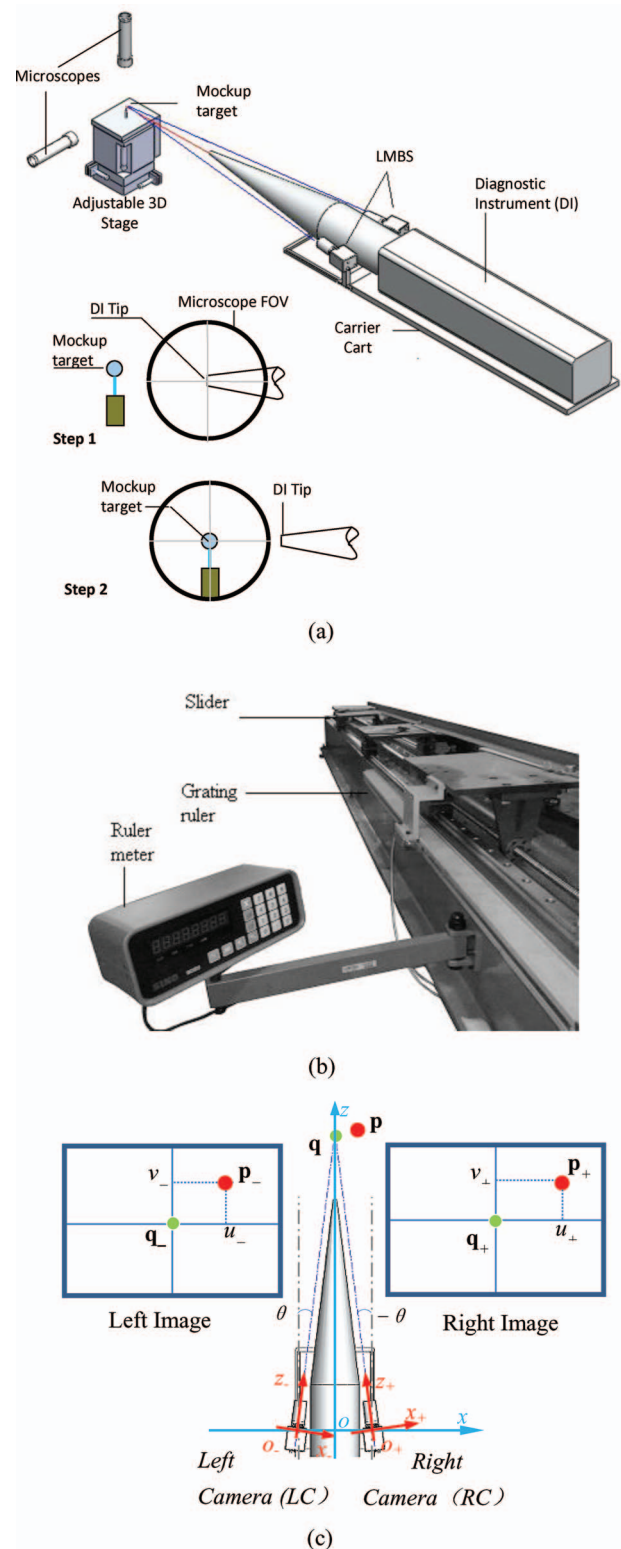


FIG. 2. (Color online) Image coordinate system. (a) Offline alignment, (b) offline alignment linear stage, and (c) the view of the binocular vision.

(spaced $2L$ apart) are mounted: $x_+y_+z_+$ and $x_-y_-z_-$ are the right camera (RC) and left camera (LC) coordinate systems, respectively; and P is a point in the XYZ reference (fixed) frame. In Fig. 2, the calibrated point q along the z axis is known with respect to xyz frame.

As viewed in the xz plane (Fig. 2), the cameras are oriented symmetrically such that their optical axes z_{\pm} meet at \mathbf{q} along the z axis,

$$\theta_{y-} = -\theta_{y+} = \theta, \quad (1a)$$

$$\mathbf{q}_{\pm} = \begin{bmatrix} 0 & 0 & \frac{z_q}{\cos \theta} \end{bmatrix}^T, \quad (1b)$$

where $0 < \theta < \pi/2$. The coordinate transformation between xyz and $x_{\pm}y_{\pm}z_{\pm}$ is given by Eq. (2):

$$\mathbf{p}_{\pm} = [x_{\pm} \ y_{\pm} \ z_{\pm}]^T = \mathbf{R}_{\pm}(\mathbf{p} - \mathbf{o}_{\pm}), \quad (2)$$

$$\text{where } \mathbf{R}_{\pm} = \begin{bmatrix} \cos \theta & 0 & \pm \sin \theta \\ 0 & 1 & 0 \\ \mp \sin \theta & 0 & \cos \theta \end{bmatrix}.$$

$$\mathbf{p} = \begin{bmatrix} \frac{x_+ + x_-}{2 \cos \theta} & \frac{y_+ + y_-}{2} & \frac{x_+ - x_-}{2 \sin \theta} - \frac{L}{\tan \theta} \end{bmatrix}^T. \quad (3)$$

As viewed by both RC and LC, \mathbf{q} coincides with the origins of the image coordinate systems (Fig. 2). Without loss of generality, both cameras are assumed identical and have the same focal length f . The transformation from the 3D camera coordinates $(x_{\pm}, y_{\pm}, z_{\pm})$ to pin-hole image coordinates (u_{\pm}, v_{\pm}) in Fig. 2 can be obtained using perspective projection (with pinhole camera) geometry,

$$\begin{bmatrix} u_{\pm} \\ v_{\pm} \end{bmatrix} = \frac{f}{z_{\pm}} \begin{bmatrix} x_{\pm} \\ y_{\pm} \end{bmatrix}. \quad (4)$$

With the aid of Fig. 3, z_{\pm} can be derived trigonometrically,

$$z_{\pm} = \frac{z_q}{\cos \theta} (1 + \Delta z_{\pm}), \quad (5)$$

where $\Delta z_{\pm} = \mp(x_{\mp} - x_{\pm} \cos 2\theta / \sin 2\theta)$. For fine-motion visual servo applications, a perturbation model based on weak-perspective about the target \mathbf{P} is derived

$$z_{\pm} \approx \frac{z_q}{\cos \theta}. \quad (6)$$

Some observations can be made from Eqs. (3) and (6) along with Fig. 3:

- When the coordinate \mathbf{p} moves along the x direction, the corresponding image points, u_+ and u_- , of both right and left cameras move in the same (positive or negative

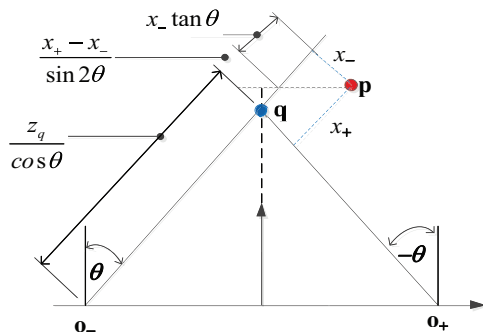


FIG. 3. (Color online) Perspective projection geometry.

u) direction. Furthermore, when \mathbf{p} is on the z axis, u_+ and u_- have the same magnitude but opposite in sign.

- Similarly, v_+ and v_- move in the same direction as \mathbf{p} moves along the y direction; and when \mathbf{p} is on the x axis, their motions in the corresponding image, v_+ and v_- , will have the same magnitude and sign.
- Unlike the x or y motion (corresponding to which the two 2D-image points move in the same u or v direction), the image points on the RC and LC move in opposite direction along u when \mathbf{p} moves along the z direction.
- Based on the above observations, a 3D image projection vector \mathbf{I} is defined to describe the target image feature in terms of position information:

$$\mathbf{I} = \begin{bmatrix} u \\ v \\ w \end{bmatrix} = \frac{1}{2} \begin{bmatrix} u_+ + u_- \\ v_+ + v_- \\ u_+ - u_- \end{bmatrix}. \quad (7)$$

Specifically, the sign of w indicates the position of \mathbf{p} relative to \mathbf{q} along the z axis,

$$\frac{1}{2}(u_+ - u_-) = w = \begin{cases} > 0 & z > z_q \\ = 0 & z = z_q \\ < 0 & z < z_q \end{cases}. \quad (8)$$

Using Eqs. (2)–(5) neglecting high order terms, \mathbf{p} can be described in terms of the right and left image coordinates

$$\mathbf{p} = [x \ y \ z]^T \approx [\mathbf{M}] \left(\frac{z_q}{f \cos \theta} \mathbf{I} + \mathbf{T}_0 \right) \quad (9)$$

$$\text{where } [\mathbf{M}] = \begin{bmatrix} 1/\cos \theta & 0 & 0 \\ 0 & 1 & 0 \\ 0 & 0 & 1/\sin \theta \end{bmatrix}; \quad \mathbf{T}_0 = \begin{bmatrix} 0 \\ 0 \\ L \cos \theta \end{bmatrix}.$$

Thus, the perturbation in the neighborhood of any target point \mathbf{P} can be expressed as

$$\Delta \mathbf{p} = [\mathbf{J}_{\text{BVS}}(\mathbf{I}, \mathbf{p})] \Delta \mathbf{I}, \quad (10)$$

where the image Jacobian $[\mathbf{J}_{\text{img}}]$ is given by

$$[\mathbf{J}_{\text{img}}] = \frac{\partial \mathbf{I}}{\partial \mathbf{p}} = \frac{z_q}{f \cos \theta} [\mathbf{M}].$$

C. Micro-motion manipulator

The operational principle of the 3-DOF manipulator (driven by three translational actuators denoted as L_1 , L_2 , and L_3) for precise radial positioning, orientation pointing, and alignment to target, along with the coordinate systems for deriving its kinematics, is illustrated in Fig. 1(b). Schematically, the bipod is treated as a plane formed by two translational actuators (L_1 and L_2) connecting to the main tube with a pair of universal joints (B_1 and B_2) and the base with ball joints (A_1 and A_2). Similarly, the three universal joints (B_1 , B_2 , and O_1) and the BVS origin O form a moving plane free to yaw and pitch about O_1 (a point fixed relative to the base denoted as a Cartesian reference frame O_0XYZ). The inverse kinematics of

the 3-DOF manipulator involves two steps: Step 1 relates the three incremental parameters (δy_m and $\delta\theta_x$ and $\delta\theta_z$ about O_1) of moving platform to $\Delta\mathbf{p}$ ($=\mathbf{p}-\mathbf{q}$), where δy_m is provided by the change in L_3 . Step 2 calculates the changes in bipod lengths (L_1 and L_2) from the specified $\delta\theta_x$ and $\delta\theta_z$ about O_1 .

1. Moving platform increments

To describe the kinematics of the moving platform, the moving frame $o_1x_my_mz_m$ is assigned at O_1 with its y_m axis pointing along the motion of linear positioner (or the z-axis of the BVS) and z_m in the normal to the plane $O_1B_1B_2$. Thus, the detected $\Delta\mathbf{p}$ ($=\mathbf{p}-\mathbf{q}$) from Eq. (10) can be expressed in $x_my_mz_m$ frame

$$\Delta\mathbf{p}_m = \begin{bmatrix} 1 & 0 & 0 \\ 0 & 0 & 1 \\ 0 & -1 & 0 \end{bmatrix} \Delta\mathbf{p}. \quad (11)$$

Given the desired and actual targets (\mathbf{q}_m and \mathbf{p}_m) in $x_my_mz_m$ frame, the two small rotations ($\delta\theta_x$ and $\delta\theta_z$ about the x_m and z_m axes, respectively) for pointing and the extension δy_m for radially positioning the moving platform can then be determined with the aid of Fig. 4 from the following relationship:

$$[\delta\mathbf{R}](\mathbf{q}_m + \delta\mathbf{p}) - \mathbf{p}_m = \Delta\mathbf{p}_m \quad (12)$$

$$\text{where } [\delta\mathbf{R}] = \begin{bmatrix} 1 & -\delta\theta_z & 0 \\ \delta\theta_z & 1 & -\delta\theta_x \\ 0 & \delta\theta_x & 1 \end{bmatrix} \text{ and } \delta\mathbf{p} = \begin{bmatrix} 0 \\ \delta y_m \\ 0 \end{bmatrix}.$$

The required increments in $\delta\theta_x$, $\delta\theta_z$, and δy_m can be derived by substituting Eq. (11) into Eq. (12) leading to

$$\begin{bmatrix} \delta\theta_x \\ \delta\theta_z \\ \delta y_m \end{bmatrix} = \frac{-1}{y_{mp}} \begin{bmatrix} 0 & 1 & 0 \\ 1 & 0 & 0 \\ x_{mp} & -z_{mp} & y_{mp} \end{bmatrix} \begin{bmatrix} \Delta x \\ \Delta y \\ \Delta z \end{bmatrix}. \quad (13)$$

2. Bipod extensions

Since the displacements of the two universal joints B_i ($i = 1, 2$) are known with respect to the moving frame, the changes in B_i in XYZ frame for given $\delta\theta_x$ and $\delta\theta_z$ can be found from Eq. (14):

$$\Delta\mathbf{P}_{Bi} = \begin{bmatrix} \Delta X_{Bi} \\ \Delta Y_{Bi} \\ \Delta Z_{Bi} \end{bmatrix} = ([\delta\mathbf{R}] - [\mathbf{I}])[\mathbf{R}_0]\mathbf{P}_{Bim}, \quad (14)$$

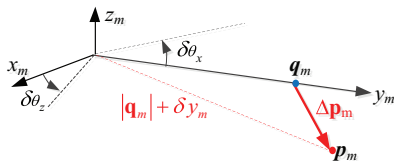


FIG. 4. (Color online) Schematics illustrating 3-DOF manipulation.

where $[\mathbf{I}]$ is the 3×3 identity matrix. Hence, the incremental length compensation needed to materialize the differential rotations is

$$\delta L_i = \begin{bmatrix} \frac{\partial L_i}{\partial X_{Bi}} & \frac{\partial L_i}{\partial Y_{Bi}} & \frac{\partial L_i}{\partial Z_{Bi}} \end{bmatrix} \Delta\mathbf{P}_{Bi}, \quad (15)$$

where $L_i = \sqrt{(X_{Bi} - X_{Ai})^2 + (Y_{Bi} - Y_{Ai})^2 + (Z_{Bi} - Z_{Ai})^2}$. Substituting Eq. (14) into Eq. (15) leads to

$$\begin{bmatrix} \delta L_1 \\ \delta L_2 \end{bmatrix} = \begin{bmatrix} m_{11} & m_{12} \\ m_{21} & m_{22} \end{bmatrix} \begin{bmatrix} \delta\theta_x \\ \delta\theta_z \end{bmatrix}, \quad (16)$$

where $m_{i1}L_i = -Z_{Bi}(Y_{Bi} - Y_{Ai}) + Y_{Bi}(Z_{Bi} - Z_{Ai})$; $m_{i2}L_i = -Y_{Bi}(X_{Bi} - X_{Ai}) + X_{Bi}(Y_{Bi} - Y_{Ai})$; and $i = 1, 2$.

3. Hybrid parallel-serial manipulator

Equations (13) and (16) can be combined and more compactly written as shown in Eq. (17):

$$\delta\mathbf{L} = \begin{bmatrix} \delta L_1 \\ \delta L_2 \\ \delta L_3 \end{bmatrix} = [\mathbf{J}_{3M}] \Delta\mathbf{p}, \quad (17)$$

$$\text{where } [\mathbf{J}_{3M}] = \frac{-1}{y_{mp}} \begin{bmatrix} m_{11} & m_{12} & 0 \\ m_{21} & m_{22} & 0 \\ x_{mp} & -z_{mp} & y_{mp} \end{bmatrix}.$$

D. Integrated V3M kinematics

The block diagram depicted in Fig. 5 illustrates the kinematic control of the V3M, where \mathbf{I}_0 is the image projection vector of the desired target location obtained from the offline alignment; and \mathbf{p}_0 is the initial image captured by the *in situ* BVS in the ICF chamber. The fine-motion vision system computed the updated \mathbf{I} from the LMBC. The desired incremental changes to drive the three linear actuators are given by Eq. (18):

$$\delta\mathbf{L} = [\delta L_1 \quad \delta L_2 \quad \delta L_3]^T = [\mathbf{J}_{3M}][\mathbf{J}_{BVS}]\Delta\mathbf{I}. \quad (18)$$

The kinematic control is best illustrated with a numerical example. The values of geometrical parameters and the randomly selected initial pose of the V3M used in simulation are summarized in Table I, where the coordinates of O_1 , A_1 , and A_2 are known in the fixed reference XYZ frame while those of B_1 and B_2 are specified with respect to local coordinate frame $x_my_mz_m$. The geometrical parameters are based on an existing LMBC-guided prototype structure developed by HUST.⁶ The forward kinematic model can be found in Ref. 6,

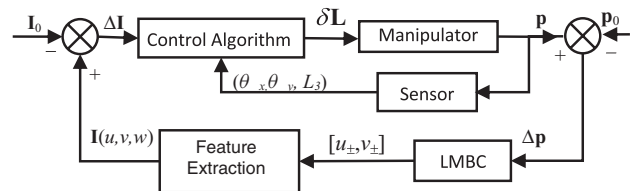


FIG. 5. Visual servo block diagram.

TABLE I. Simulation input parameters.

Coordinates (m)		Cameras (LMBC)	
In fixed [X, Y, Z] frame		L (mm)	200
A_1	$[-0.750, -5.2467, 0]$	f (mm)	160
A_2	$[0.750, -5.2467, 0]$	θ ($^\circ$)	20
O_1	$[0, 0, 1.20]$	Frame rate (fps)	10
In moving $[x_m, y_m, z_m]$ frame		Other geometry	
B_1	$[-0.441, -5.2465, 0]$	L_3 (mm)	1940.5
B_2	$[0.441, 5.2465, 0]$		
O	$[0, 1.950, 0]$		
Initial conditions			
Target position in fix frame (m)		$[0, 2.5, 1.2]$	
Manipulator orientation (θ_X, θ_Z)		$(0.1^\circ, -0.2^\circ)$	

an English version is briefly summarized in the Appendix for completeness.

From the current pose, the three actuating lengths of the manipulator can be calculated from inverse kinematic model (16), which moves the LMBC to capture new images and compute \mathbf{I} to characterize the target coordinate. The difference between \mathbf{I} and the desired target \mathbf{I}_0 (from offline alignment), along with the measurements $(\delta\theta_x, \delta\theta_z, \text{ and } L_3)$ that characterize the pose of the manipulator, is used as a basis to point, position, and align to target. Figure 5 shows the simulated deviations $(\delta u, \delta v, \text{ and } \delta w)$ and their resultant $|\delta \mathbf{I}|$.

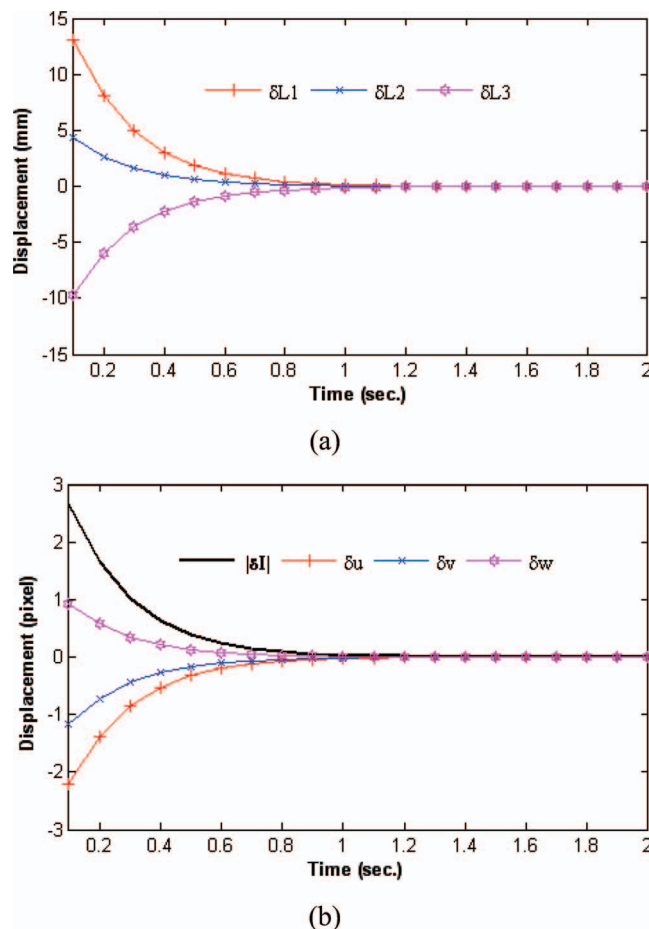


FIG. 6. (Color online) (a) and (b) Simulation results.

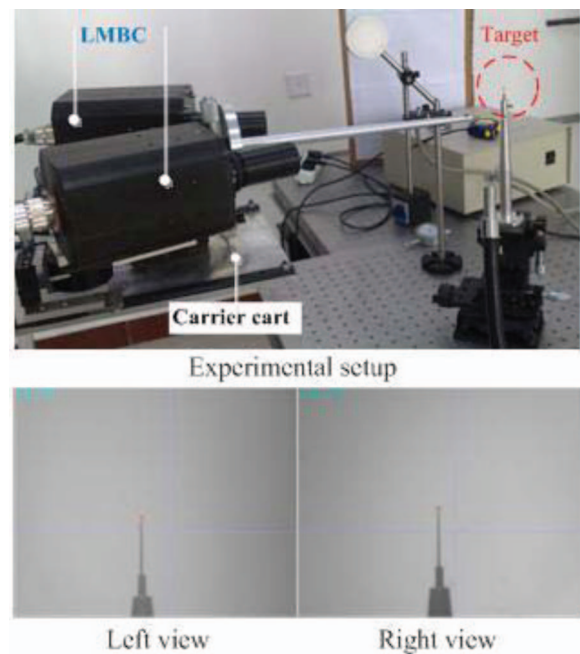


FIG. 7. (Color online) LMBC and images.

Simulated results in Fig. 5 show the displacements of the limbs and the IPV, where δu , δv , and δw denote the deviation of the current IPV from desired; and $|\delta \mathbf{I}|$ is the deviated length of IPV. As shown in Fig. 6(a), the L_1 and L_2 are in opposite direction of L_3 . L_1 experiences a larger change than L_2 indicating that the DIM simultaneously rotates counterclockwise about the Z-axis and clockwise about the X-axis during compensation.

III. EXPERIMENTAL RESULTS

The image acquisition/processing system includes two TM-1405 Gigabit Ethernet Cameras and an industrial PC (IntelP4 2.6G CPU with 1G RAM). Communication with the control system is established through Ethernet. The cameras (each with a $0.4\times$ lens magnification) are spaced 400 mm apart and sealed in an enclosed environment. Both of their axes converge towards the target about 500 mm away from them. The diameter of the work target is $200 \mu\text{m}$. Image features are detected with sub-pixel precision. Given the simplicity of the image, the error is less than 0.2 pixels. These settings are employed for prototype verification; it is expected further optimization can be achieved based on the application needs.

Experiments were performed with the above-mentioned DIM prototype and a fast template-matching algorithm (called local entropy difference⁷) for calculating the target center in the image. Figure 7 shows the LMBC and the target left and right images where the crosses "+" represent the desired position captured using the offline aligning stage. Experimental results are displayed in Fig. 8 showing the target position in the two images and the IPV that approaches to zero in scores of seconds implying that the instrument has been located at the desired position after the self-positioning. As the manipulator is relatively heavy, the speeds of limbs extension were restricted; as a result, self-positioning took about 10 seconds to approach the steady state and maintain stability.

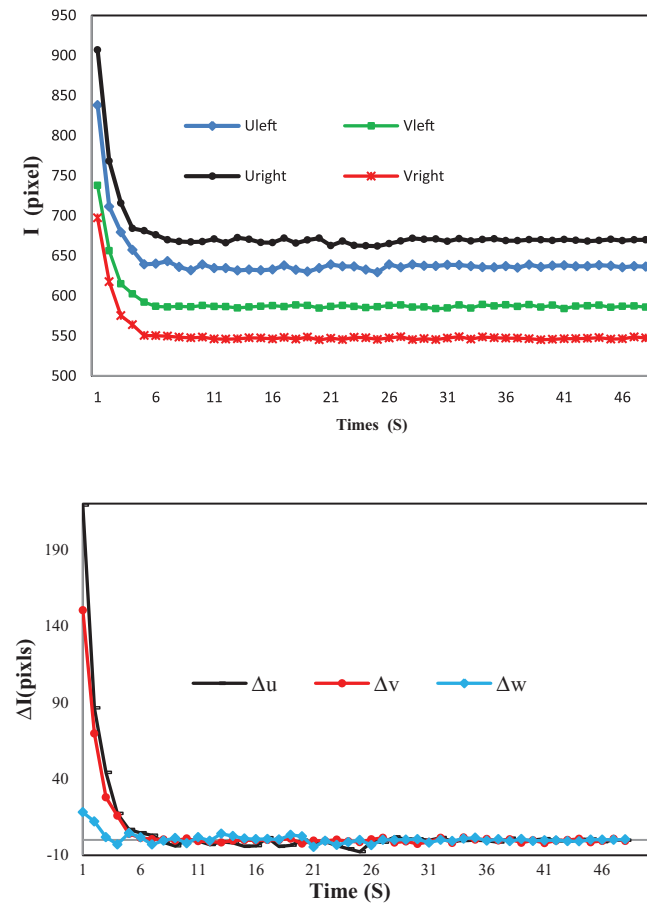


FIG. 8. (Color online) Experimental results.

IV. CONCLUSION

A new method for instrument positioning for ICF experiment has been presented, which employs a LMBC and a 3-DOF micromanipulator. The LMBC generates an image displacement vector, which is correlated with the limbs length of the micromanipulator, to estimate the position displacement in 3D space. With the visual feedback, the manipulator enforces the instrument approaching to its desired position. The experiment results show that the positioning accuracy of this system is within $25 \mu\text{m}$. Further work on the effects of structural dynamics on the performance of this method is being investigated.

ACKNOWLEDGMENTS

The authors wish to thank Junfeng Wang and Wuxin Lai for close collaboration. Wei Wang gratefully acknowledges financial support from China Scholarship Council for his visiting at Georgia Institute of Technology and wishes to thank the AIMRL group for valuable discussion.

APPENDIX: INVERSE KINEMATICS AND FORWARD KINEMATICS

The inverse kinematics of the manipulator in Eqs. (A1) and (A2) map the actuating lengths for a specified end point

position and orientation of the moving frame, respectively,

$$L_3 = |P_o - P_{o1}| = y_{mo}, \quad (\text{A1})$$

where $P_o(x_{mo}, y_{mo}, z_{mo})$ is the current position of the end effector and P_{o1} is the position of initial point O_1 . The orientation of the moving platform (represented by rotational matrix R) can be obtained with the aid of sensors. As joints position ($\mathbf{p}_{mA}, \mathbf{p}_{mB}$) and R known, the length of two limbs can be computed. That is

$$L_{1,2} = \sqrt{\mathbf{p}_{mA,mB}^T [\mathbf{R}]^T [\mathbf{R}] \mathbf{p}_{mA,mB} + \mathbf{P}_{A0,B0} \mathbf{P}'_{A0,B0} - 2\mathbf{P}_{A0,B0} \mathbf{R}' \mathbf{p}_{mA,mB}} \quad (\text{A2})$$

$$[\mathbf{R}] = \begin{bmatrix} \cos \theta_Z & -\sin \theta_Z & 0 \\ \cos \theta_X \sin \theta_Z & \cos \theta_X \cos \theta_Z & -\sin \theta_X \\ \sin \theta_X \sin \theta_Z & \sin \theta_X \cos \theta_Z & \cos \theta_X \end{bmatrix}.$$

The forward kinematics determines the pose of the moving platform from a known set of the actuated inputs. For the manipulator shown in Fig. 1, the three linear actuating inputs that L_1, L_2 , and L_3 and the unknown pose is described by the vector $P_o(X_o, Y_o, Z_o)$. Expanding Equation (A2) and rearranging the terms yields

$$\begin{cases} \cos \theta_Z (1 + \cos \theta_X \kappa_1) = \kappa_3 \\ \sin \theta_Z (1 + \cos \theta_X \kappa_2) = \kappa_4 \end{cases}, \quad (\text{A3})$$

where $\kappa_1 = (y_{mB1} Y_{A1} / x_{mB1} X_1)$, $\kappa_2 = (y_{mB1} X_{A1} / x_{mB1} Y_{A1})$, $\kappa_4 = -(L_{\text{left}}^2 - L_{\text{right}}^2 / 4x_{mB1} Y_{A1})$ and $\kappa_3 = (1/2x_{mB1} X_{A1})[(x_{mB1}^2 + y_{mB1}^2 + X_{A1}^2 + Y_{A1}^2) - (L_{\text{left}}^2 + L_{\text{right}}^2)/2]$.

Equation (A3) can be rewritten as

$$\lambda_1 \cos^4 \theta_X + \lambda_2 \cos^3 \theta_X + \lambda_3 \cos^2 \theta_X + \lambda_4 \cos \theta_X - \lambda_5 = 0, \quad (\text{A4})$$

where $\lambda_1 = \kappa_1^2 \kappa_2^2$, $\lambda_2 = 2(\kappa_1 \kappa_2^2 + \kappa_1^2 \kappa_2)$, $\lambda_3 = (\kappa_1^2 + \kappa_2^2 + 4\kappa_1 \kappa_2 - \kappa_2^2 \kappa_3^2 - \kappa_1^2 \kappa_4^2)$, $\lambda_4 = 2(\kappa_2 + \kappa_1 - \kappa_2 \kappa_3^2 - \kappa_1 \kappa_4^2)$, and $\lambda_5 = -(\kappa_3^2 + \kappa_4^2 - 1)$.

Equation (A4) is a quartic equation which can be solved for θ_X in the range of $[-\pi/2, \pi/2]$. Once θ_X is known, the complete solution to the forward kinematics can be obtained in closed form from Equation (A3).

¹W. J. Hibbard, M. D. Landon, M. D. Vergino, and F. D. Lee *Rev. Sci. Instrum.* **72**, 530 (2001).

²K. B. Fournier, J. Celeste, V. Rekow, D. R. Bopp, M. J. May, J. H. Fisher, R. Horton, C. D. Newlander, P. Jenkins, and K. Trautz, *Rev. Sci. Instrum.* **81**, 075113 (2010).

³H. Peng, X. M. Zhang, X. Wei, W. Zheng, F. Jing, Z. Sui, D. Fan, and Z. Lin, *Proc. SPIE* **3492**, 25 (1999).

⁴Z. Li, X. Jiang, S. Liu, T. Huang, J. Zheng, J. Yang, S. Li, L. Guo, X. Zhao, H. Du, T. Song, R. Yi, Y. Liu, S. Jiang, and Y. Ding, *Rev. Sci. Instrum.* **81**, 073504 (2010).

⁵X. Kang, J. Chen, C. Deng, Z. Liu, X. Zhan, and M. Chen, [Rev. Sci. Instrum.](#) **79**, 086109 (2008).

⁶W. Wang, J. Wang, T. Shi, and W. Lai, [High Power Laser and Particle Beams](#), **22**, 1259 (2010) (in Chinese).

⁷W. Lai, W. Wang, B. Huang, H. Ren and T. Shi, in *Proceedings of the 2nd International Congress on Image and Signal Processing, Tianjin 2009*, edited by P. Qiu, C. Yiu, H. Zhang, and X. Wen (IEEE, Piscataway, NJ, 2009), pp. 1–5.